Complex scaled nonlocalized cluster model for ^{8}Be

Hantao Zhang,[1,*] Dong Bai,[2,†] Zhen Wang,[1,‡] and Zhongzhou Ren[1,3,§]
[1]*School of Physics Science and Engineering, Tongji University, Shanghai 200092, China*
[2]*College of Science, Hohai University, Nanjing 211100, Jiangsu, China*
[3]*Key Laboratory of Advanced Micro-Structure Materials, Ministry of Education, Shanghai 200092, China*

(Received 1 March 2022; accepted 3 May 2022; published 26 May 2022)

The nonlocalized cluster model provides a new perspective for describing nuclear cluster effects and has been successfully applied in the study of cluster structures in bound states, scattering states, and also resonant states. However, there is still some room for development when dealing with resonance problems with this new model. The complex scaling method (CSM) is an important method in research of the resonant states. We combine CSM with the nonlocalized cluster model [B. Zhou *et al.*, Phys. Rev. Lett. **110**, 262501 (2013)] for the first time, and such combination provides a new way to study the resonance in the nonlocalized cluster model. Here, we apply the CSM to ^{8}Be as a simple example to illustrate its usages and advantages, while pointing out that the generalization to more complicated cluster systems is also natural.

DOI: 10.1103/PhysRevC.105.054317

I. INTRODUCTION

In nuclear many-body problems the cluster structures are very important and have been widely studied through both experimental and theoretical approaches, among which the nonlocalized cluster model [1–6] is a crucial one for describing the cluster phenomenon. In the traditional image of the localized cluster model, the clusters are located in fixed positions, while in the nonlocalized model, they can move in space with the exchange of nucleons and satisfy the Pauli principle. This model has been applied to study nuclear structures of bound states and quasi-bound states (long-lived resonant states) in various light nuclei, including ^{6}He [7], ^{8}Be [8,9], ^{9}Be [10], ^{10}Be [11], ^{11}Be [12], ^{9}B [13], ^{10}B [14], ^{10}C [14], ^{12}C [1,9,15–19], ^{16}O [1,9,15,18,20], ^{20}Ne [21–24], and so on. However, at present there still exist some shortcomings when dealing with resonance problems with this new model.

The complex scaling method [25] (CSM) as an important method in research of the resonant states has been successfully applied in few-body resonance and nonresonant continuum states, as well as scattering states studied with Lippmann-Schwinger equation, which can deal with some nuclear reaction problems. However, in the cluster models the applications of this method is still relatively rare.

We combine CSM with the nonlocalized cluster model for the first time, and such combination provides a new way to study the resonance in the nonlocalized cluster model. Several methods have already been applied for studying resonance states within the cluster model, for example, the R-matrix method [26–30], the Analytic continuation in the coupling constant (ACCC) method [31,32], etc., where the R-matrix method determines the location and width resonance state by calculating the phase shift-energy curve, while the ACCC method adds an artificial attractive pseudopotential $\delta \times V$ (δ is a constant) into the original Hamiltonian and determines the resonance state by adjusting the coupling constant δ. The CSM utilized in this work is a direct method, which associates the resonance position and width directly to the real and imaginary parts of the complex energy, and they are obtained simultaneously by solving a complex scaled Schrödinger equation. In Sec. II we will give a more detailed description of the complex scaling method and show how to combine it with the nonlocalized cluster model.

As a simple test here we would like to consider the resonances of ^{8}Be, which is considered to have a strong α cluster effect. Such an α-α system has rich physical properties and is important for understanding many crucial nuclear reactions in astrophysics. The low-lying resonances of ^{8}Be have been measured; we will use them to confirm and validate our method. Various theoretical works have been proposed to study different aspects of the nature of ^{8}Be, such as the resonating group method (RGM) [33,34], the generator coordinate method (GCM) [26,35,36], the Tohsaki-Horiuchi-Schuck-Röpke (THSR) wave function [8,9], the cluster effective field theory [37,38], the complex-scaled cluster model [39–42], and so on. In this work we choose the THSR wave function as the basis function in the nonlocalized cluster; model, the THSR wave function was originally introduced to illustrate the 3α-condensate-like characteristics of the Hoyle state (0_2^+ state) of ^{12}C [6] and has been developed successfully to study more complicated systems containing more α clusters. With all these successful experiences of studying the α-α and more complicated cluster systems we are able to extend our method further to the three and more α

*zhang_hantao@foxmail.com
†dbai@hhu.edu.cn
‡wang_zhen@tongji.edu.cn
§Corresponding author: zren@tongji.edu.cn

systems, which may contain exotic structures such as gaslike α condensates [1], linear chain structure [15], etc. Also, these exotic structures may correspond some more interesting characteristics of the resonance states.

In Sec. II we formulate the THSR framework of the general cluster model and then specify it for ^{8}Be. The interaction model and the relevant matrix element are also formulated in this section but the details are given in the Appendix. In the last part of Sec. II we introduce the complex scaling method and apply it to the THSR framework. Eventually we provide the GCM as a comparison with THSR and make a computational test using GCM. We demonstrate the relevant numerical results in Sec. III and discuss them in the final section. Also, in the final section we give a brief description of the possible extensions and prospects of our approach. Several computational details about the THSR wave function are all given in the Appendix.

II. THEORETICAL FORMALISM

The THSR wave function can be expressed as a superposition of Brink wave functions, which are used in the generator coordinate method, $\Phi^B(\mathbf{R}_1, \ldots, \mathbf{R}_n)$ [8]:

$$\Phi_{n\alpha}(\beta_x, \beta_y, \beta_z) = \int d^3R_1 \cdots d^3R_n \exp\left\{-\sum_{i=1}^{n}\left(\frac{R_{ix}^2}{\beta_x^2}+\frac{R_{iy}^2}{\beta_y^2}+\frac{R_{iz}^2}{\beta_z^2}\right)\right\}\Phi^B(\mathbf{R}_1, \cdots, \mathbf{R}_n),$$
$$\Phi^B(\mathbf{R}_1, \cdots, \mathbf{R}_n) = \det\{\phi_{0s}(\mathbf{r}_1-\mathbf{R}_1)\chi_{\sigma_1\tau_1}\cdots\phi_{0s}(\mathbf{r}_{4n}-\mathbf{R}_n)\chi_{\sigma_{4n}\tau_{4n}}\}, \tag{1}$$

where $\chi_{\sigma\tau}$ is the spin-isospin wave function. But the wave function above corresponds to the intrinsic state of the cluster condensation without certain angular momentum; therefore we need to make the angular momentum projection as follows:

$$\begin{aligned}\Phi^J_{n\alpha}(\beta_x, \beta_y, \beta_z) &= \int d\Omega\, D^{J*}_{MK}(\Omega)\hat{R}(\Omega)\Phi_{n\alpha}(\beta_x, \beta_y, \beta_z)\\ &= \int d\Omega\, D^{J*}_{MK}(\Omega)\int d^3R_1\cdots d^3R_n \exp\left(-\sum_{i=1}^{n}\sum_{k=x,y,z}\frac{R_{ik}^2}{\beta_k^2}\right)\Phi^B(R^{-1}(\Omega)\mathbf{R}_1, \ldots, R^{-1}(\Omega)\mathbf{R}_n)\\ &= \int d\Omega\, D^{J*}_{MK}(\Omega)\int d^3R_1\cdots d^3R_n \exp\left(-\sum_{i=1}^{n}\sum_{k=x,y,z}\frac{(R(\Omega)\mathbf{R}_i)_k^2}{\beta_k^2}\right)\Phi^B(\mathbf{R}_1, \ldots, \mathbf{R}_n),\end{aligned} \tag{2}$$

where Ω is the Euler angle, D^J_{MK} is the Wigner D function, $\hat{R}(\Omega)$ is the rotation operator, and $R(\Omega)$ represents the 3×3 rotation matrix corresponding to the rotation operator $\hat{R}(\Omega)$. Here we make use of the relation $\phi_{0s}(R(\Omega)\mathbf{r}-\mathbf{R}) = \phi_{0s}(\mathbf{r}-R^{-1}(\Omega)\mathbf{R})$, which can be obtained obviously from the expression of the $0s$ harmonic oscillator wave function (Gaussian wave packet).

By transforming $\mathbf{R}_1$ and $\mathbf{R}_2$ into the center-of-mass coordinate $\mathbf{R}_G$ and the relative coordinate $\mathbf{R}$,

$$\mathbf{R}_1 = \mathbf{R}_G + \mathbf{R}/2, \mathbf{R}_2 = \mathbf{R}_G - \mathbf{R}/2, \tag{3}$$

the THSR wave function of the 2α system is written as

$$\begin{aligned}\Phi_{2\alpha}(\beta_x, \beta_y, \beta_z) &= \int d^3R_1 d^3R_2 \exp\left\{-\sum_{i=1}^{2}\left(\frac{R_{ix}^2}{\beta_x^2}+\frac{R_{iy}^2}{\beta_y^2}+\frac{R_{iz}^2}{\beta_z^2}\right)\right\}\Phi^B(\mathbf{R}_1, \mathbf{R}_2)\\ &= 4!\left(\frac{4}{\pi b^2}\right)^{3/2}\int d^3R_G \exp\left\{-\left(\sum_{k=x,y,z}\frac{2R_{Gk}^2}{\beta_k^2}\right)-\frac{4}{b^2}(\mathbf{X}_G-\mathbf{R}_G)^2\right\}\\ &\quad\times\int d^3R \exp\left(-\sum_{k=x,y,z}\frac{R_k^2}{2\beta_k^2}\right)\mathcal{A}\left[\exp\left\{-\frac{1}{b^2}(\mathbf{r}-\mathbf{R})^2\right\}\phi(\alpha_1)\phi(\alpha_2)\right],\end{aligned} \tag{4}$$

where $\mathbf{X}_G = (\mathbf{X}_1+\mathbf{X}_2)/2$ and $\mathbf{r} = \mathbf{X}_1 - \mathbf{X}_2$; here $\mathbf{X}_i$ denotes the center-of-mass coordinate of the ith α cluster α_i. If we let $\mathbf{R}_G$ be zero and so avoid the integration of $\mathbf{R}_G$ in Eq. (4), we obtain a new wave function denoted by $\Psi_{2\alpha}(\beta_x, \beta_y, \beta_z)$:

$$\begin{aligned}\Psi_{2\alpha}(\beta_x, \beta_y, \beta_z) &= 4!\left(\frac{4}{\pi b^2}\right)^{3/2}\exp\left(-\frac{4}{b^2}\mathbf{X}_G^2\right)\int d^3R \exp\left(-\sum_{k=x,y,z}\frac{R_k^2}{2\beta_k^2}\right)\mathcal{A}\left[\exp\left\{-\frac{1}{b^2}(\mathbf{r}-\mathbf{R})^2\right\}\phi(\alpha_1)\phi(\alpha_2)\right]\\ &= \int d^3R \exp\left(-\sum_{k=x,y,z}\frac{R_k^2}{2\beta_k^2}\right)\Phi^B(\mathbf{R}/2, -\mathbf{R}/2).\end{aligned} \tag{5}$$

By neglecting the center-of-mass wave function in Eq. (5) we can define a internal wave function, which is denoted by $\Phi'_{2\alpha}(\beta_x, \beta_y, \beta_z)$ [the constant factor in equation (5) is not important]:

$$\Phi'_{2\alpha}(\beta_x, \beta_y, \beta_z) = \int d^3R \exp\left(-\sum_{k=x,y,z}\frac{R_k^2}{2\beta_k^2}\right)\mathcal{A}\left[\exp\left\{-\frac{1}{b^2}(\mathbf{r}-\mathbf{R})^2\right\}\phi(\alpha_1)\phi(\alpha_2)\right]. \tag{6}$$

In this work we only handle the case of axially symmetric deformation with the z axis being the symmetry axis, namely $\beta_x = \beta_y \neq \beta_z$. In this case, we can do the replacements as follows in the angular momentum projection:

$$\begin{aligned}&\int d\Omega \Longrightarrow 4\pi^2 \int d\cos(\zeta), \quad D^{J*}_{MK}(\Omega) \Longrightarrow d^J_{00}(\zeta) = P_J(\cos(\zeta)),\\ &\hat{R}(\Omega) \Longrightarrow \hat{R}_y(\zeta), \quad R(\Omega) \Longrightarrow R_y(\zeta),\end{aligned} \tag{7}$$

where $P_J(\cos(\zeta))$ is the Legendre polynomial and we will use it instead of $d^J_{00}(\zeta)$ in the following formulations. The correct internal wave function with good angular momentum can be defined as

$$\Phi'^J_{2\alpha}(\beta_x = \beta_y, \beta_z) = \int d\cos(\zeta) P_J(\cos(\zeta))\hat{R}_y(\zeta)\Phi'_{2\alpha}(\beta_x = \beta_y, \beta_z). \tag{8}$$

The matrix element of a translationally invariant operator $\hat{O}$ with the spin projected wave function $\Phi'^J_{2\alpha}(\beta_x = \beta_y, \beta_z)$ is calculated as

$$\frac{\langle\Phi'^J_{2\alpha}(\beta_x = \beta_y, \beta_z)|\hat{O}|\Phi'^J_{2\alpha}(\beta_x = \beta_y, \beta_z)\rangle}{\langle\Phi'^J_{2\alpha}(\beta_x = \beta_y, \beta_z)|\Phi'^J_{2\alpha}(\beta_x = \beta_y, \beta_z)\rangle} = \frac{\int d\cos(\zeta) P_J(\cos(\zeta))\langle\Phi'_{2\alpha}|\hat{O}\hat{R}_y(\zeta)|\Phi'_{2\alpha}\rangle}{\int d\cos(\zeta) P_J(\cos(\zeta))\langle\Phi'_{2\alpha}|\hat{R}_y(\zeta)|\Phi'_{2\alpha}\rangle}. \tag{9}$$

In the actual calculation we want to use an expression like Eq. (5) instead of (6) to determine the matrix elements because of the simpler technique of GCM. However, on account of the center-of-mass motion in the wave function $\Psi_{2\alpha}(\beta_x = \beta_y, \beta_z)$, the Hamiltonian H we use in this work is written as

$$H = T - T_G + V_N + V_C, \tag{10}$$

where T is the total kinetic energy, T_G is the center-of-mass kinetic energy, V_N is the effective two-body nuclear interaction energy, and V_C is the Coulomb interaction energy. We adopt the Volkov No. 1 potential as the effective two-body nuclear potential, which has the form [43]

$$V_N = \frac{1}{2}\sum_{i\neq j}^{8}\{(1-M) - MP_\sigma P_\tau\}_{ij}\sum_{n=1}^{2}V_n \exp\left(-\frac{r_{ij}^2}{a_n^2}\right), \tag{11}$$

where the parameters V_n and a_n are $a_1 = 1.60$ fm, $a_2 = 0.82$ fm, $V_1 = -83.34$ MeV, $V_2 = 144.86$ MeV and M is the Majorana exchange parameter. The Coulomb interaction can be written as

$$V_C = \frac{1}{2}\sum_{i\neq j}^{8}\left(\frac{1}{2}+t_{zi}\right)\left(\frac{1}{2}+t_{zj}\right)\frac{e^2}{r_{ij}}, \tag{12}$$

where the isospin z component equals $t_z = +1/2$ for the proton and $t_z = -1/2$ for the neutron. Consequently the matrix element for the spin projected $\Psi_{2\alpha}(\beta_x = \beta_y, \beta_z)$ has the same form as Eq. (9):

$$\frac{\langle\Psi^J_{2\alpha}(\beta_x = \beta_y, \beta_z)|\hat{O}|\Psi^J_{2\alpha}(\beta_x = \beta_y, \beta_z)\rangle}{\langle\Psi^J_{2\alpha}(\beta_x = \beta_y, \beta_z)|\Psi^J_{2\alpha}(\beta_x = \beta_y, \beta_z)\rangle} = \frac{\int d\cos(\zeta) P_J(\cos(\zeta))\langle\Psi_{2\alpha}|\hat{O}\hat{R}_y(\zeta)|\Psi_{2\alpha}\rangle}{\int d\cos(\zeta) P_J(\cos(\zeta))\langle\Psi_{2\alpha}|\hat{R}_y(\zeta)|\Psi_{2\alpha}\rangle}, \tag{13}$$

where

$$\begin{aligned}\Psi^J_{2\alpha}(\beta_x = \beta_y, \beta_z) &= \int d\cos(\zeta) P_J(\cos(\zeta))\hat{R}_y(\zeta)\Psi_{2\alpha}(\beta_x = \beta_y, \beta_z)\\ &= \int d\cos(\zeta) P_J(\cos(\zeta))\hat{R}_y(\zeta)\int d^3R \exp\left(-\sum_{k=x,y,z}\frac{R_k^2}{2\beta_k^2}\right)\Phi^B(\mathbf{R}/2, -\mathbf{R}/2)\\ &= \int d\cos(\zeta) P_J(\cos(\zeta))\int d^3R \exp\left(-\sum_{k=x,y,z}\frac{(R_y(\zeta)\mathbf{R})_k^2}{2\beta_k^2}\right)\Phi^B(\mathbf{R}/2, -\mathbf{R}/2).\end{aligned} \tag{14}$$

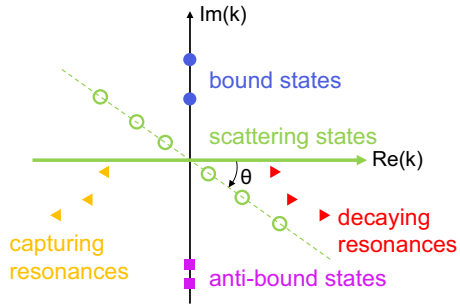

FIG. 1. The schematic momentum spectrum of a transformed Hamiltonian $H(\mathbf{r},\theta)$.

Applying the method of complex scaling to a single-particle problem, we can obtain a similarity transformation from the conventional Hamiltonian as follows:

$$H(\mathbf{r},\theta) = U(\theta)H(\mathbf{r})U(\theta)^{-1}, \tag{15}$$

where U(θ) is defined as

$$U(\theta)f(\mathbf{r}) = \exp\left(i\frac{3}{2}\theta\right)f(\mathbf{r}\exp(i\theta)), \quad 0 < \theta < \pi/2. \tag{16}$$

With this scaled Hamiltonian a corresponding complex Schrödinger equation can be written as

$$H(\mathbf{r},\theta)\Psi(\mathbf{r},\theta) = E(\theta)\Psi(\mathbf{r},\theta). \tag{17}$$

According to the so-called ABC theorem [44,45], after this transformation a bound state eigenvalue of H remains still an eigenvalue of $H(\theta)$; a resonance pole $E - i\Gamma/2$ of the Green operator of H is an eigenvalue of $H(\theta)$; the continuous spectrum of H is rotated down into the complex plane by the angle θ (the schematic momentum spectrum is shown in Fig. 1). More details about the momentum spectrum can be found in [46,47]. Additionally an important point is that the wave functions of resonant states become square integrable, therefore the whole variety of approximation methods developed for bound states can be exactly applied to resonant states. For example, one can expand over a set of linearly independent real square-integrable functions $\chi_i(\mathbf{r})$ with complex coefficients $c_i(\theta)$ to approximate the wave function $\Psi(\mathbf{r},\theta)$,

$$\Psi(\mathbf{r},\theta) = \sum_{i=1}^{N} c_i(\theta)\chi_i(\mathbf{r}), \tag{18}$$

where the unknown coefficients $c_i(\theta)$ can be determined by a generalized variational principle:

$$\delta\left[\int d\mathbf{r}\bar{\Psi}_i(\mathbf{r},\theta)^* H(\mathbf{r},\theta)\Psi_j(\mathbf{r},\theta) \Big/ \int d\mathbf{r}\bar{\Psi}_i(\mathbf{r},\theta)^*\Psi_j(\mathbf{r},\theta)d\mathbf{r}\right] = 0. \tag{19}$$

The bar on the wave function means the complex conjugate of the angular factor. For coefficients we obtain the matrix function

$$\sum_{j=1}^{N}(H_{ij}(\theta) - EN_{ij})c_j(\theta) = 0, \tag{20}$$

where

$$H_{ij}(\theta) = \int d\mathbf{r}\bar{\chi}_i(\mathbf{r})^* H(\mathbf{r},\theta)\chi_j(\mathbf{r}),$$
$$N_{ij} = \int d\mathbf{r}\bar{\chi}_i(\mathbf{r})^*\chi_j(\mathbf{r}). \tag{21}$$

Equivalently these matrix elements can be expressed as matrix elements of the unrotated real operator $H(\mathbf{r})$ or 1 between the basis functions after complex rotation:

$$\chi_i(\mathbf{r},\theta) = U(\theta)^{-1}\chi_i(\mathbf{r}) = \exp\left(-i\frac{3}{2}\theta\right)\chi_i(\mathbf{r}\exp(-i\theta)). \tag{22}$$

Since we expand the wave function over finite basis functions to solve the Schrödinger equation approximately, the ABC theorem is also fulfilled only approximately. A direct consequence is that no eigenvalue which is completely independent of θ exists, and the energy of the resonant state will also move along trajectories in the complex plane as a function of θ. A natural but heuristic criterion of estimation for a resonance energy is the minimal rate of change with respect to θ. Actually this had been suggested and confirmed in many papers; the procedure above also can be justified by an extension of the virial theorem [48].

In our case the complex scaling can be introduced by letting the generator coordinate be $R_\theta = e^{i\theta}R$ in the GCM framework or letting the deformation parameter be $\beta_\theta = e^{i\theta}\beta$ in THSR framework. In detail the complex wave function of GCM reads $\Phi^B(e^{i\theta}\mathbf{R}_1,\ldots,e^{i\theta}\mathbf{R}_n)$, while the complex THSR wave function can be written as

$$\int d^3R_1\cdots d^3R_n \exp\left(-\sum_{k=x,y,z}\frac{\mathbf{R}_k^2}{(e^{i\theta}\beta_k)^2}\right)\Phi^B(\mathbf{R}_1,\ldots,\mathbf{R}_n).$$

In addition, we need to use the c-product (bi-orthogonal product) instead of the normal inner product to calculate the matrix elements [49].

If we use complex scaled operators instead of complex scaled wave functions, the calculation scheme becomes different but equivalent:

$$T \to \exp(-2i\theta)T,$$
$$V(\mathbf{r}) \to V(\mathbf{r}\exp(i\theta)),$$
$$b \to \exp(-i\theta)bm \tag{23}$$

and then the generator coordinates $\mathbf{R}$ and deformation parameters β remain real for GCM and THSR frameworks, respectively. In this way the schemes of the calculation in two frameworks are unified and the only difference is the superposition parameter of the wave functions.

III. NUMERICAL RESULTS

The binding energy of a single alpha particle which is independent of the Majorana parameter M of the Volkov No. 1 force takes the lowest value E_α=−27.08 MeV for the parameter b = 1.37 fm [8]. We want to select a more appropriate value for parameter b and fix it in the subsequent calculations,

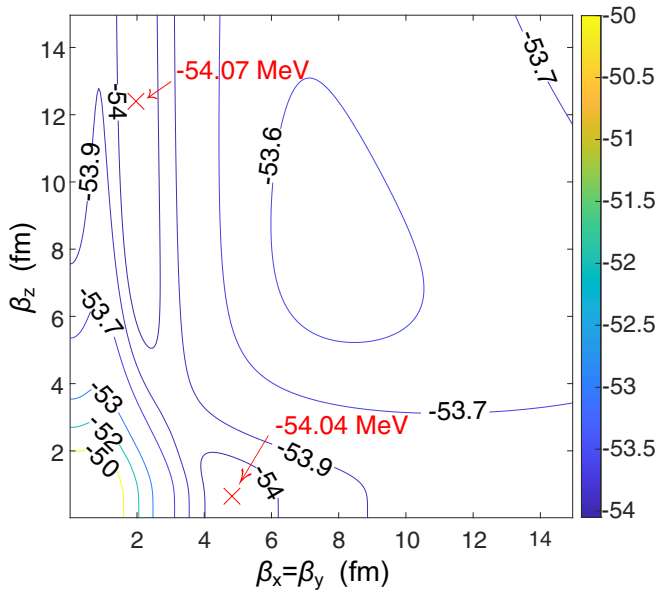

FIG. 2. Contour map of the energy surface of the ground state (0^+ state) of ^{8}Be in the two-parameter space, $\beta_x = \beta_y$ and β_z . The locations of the two minimal values have been marked in the figure. A single THSR wave function gives the lowest energy -54.07 MeV at $\beta_x = \beta_y \approx 2.0$ fm and $\beta_z \approx 12.4$ fm. Another local minima -54.04 MeV at $\beta_x = \beta_y \approx 4.8$ fm and $\beta_z \approx 0.7$ fm is very close to the lowest energy.

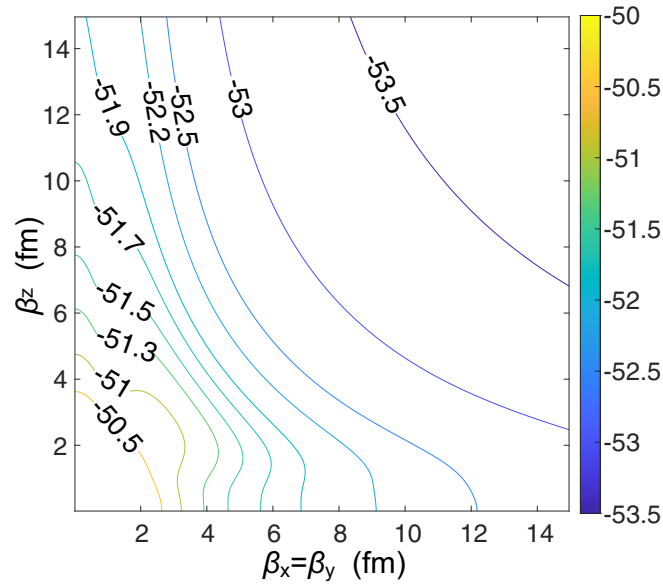

FIG. 3. Contour map of the energy surface of the 2^+ state of ^{8}Be in the two-parameter space, $\beta_x = \beta_y$ and β_z.

therefore at first we can calculate the spherical state with two parameters b and $\beta_x = \beta_y = \beta_z = \beta$, which is without the spin projection. After calculation we find that the value of parameter b at the energy minimum is about 1.36 fm, which is a little bit smaller than the b value of the free alpha particle. We fix the value of parameter b to 1.36 fm in the subsequent calculations and only change the parameter β to plot the contour map of energy. As the strength of the Majorana parameter chosen for ^{8}Be, we adopt the value $M = 0.573$, because with this value the lowest binding energy of the 0^+ state takes the value -54.07 MeV as seen in Fig. 2; that is, about 0.10 MeV higher than the two-alpha threshold energy, $2E_\alpha = -54.17$ MeV, which is consistent with the experimental value 0.0918 MeV above the 2α threshold.

It can be seen from Fig. 2 that, for the 0^+ state, a single THSR wave function gives the lowest energy, -54.07 MeV, when the deformation parameter β is taken as $\beta_x = \beta_y \approx 2.0$ fm and $\beta_z \approx 12.4$ fm. In addition to this point, there is a local minima -54.04 MeV when the parameter is $\beta_x = \beta_y \approx 4.8$ fm and $\beta_z \approx 0.7$ fm, which is very close to the lowest energy. The excited states above the 0^+ state have no energy minima at the present parameters, so we do not discuss them further than the corresponding energy contour maps shown in Figs. 3 and 4. Since the THSR wave function as a superposition of the Brink wave function is only an approximate solution, we can use more than one THSR wave function to obtain more accurate ground state energy, but of course the contribution at these two local minima is the largest. Figure 5 shows the convergence curve of the ground state energy after superimposing multiple THSR wave functions, and for comparison we also plot such curve obtained from superimposing multiple GCM wave functions. The energy converges to about -54.074 MeV when there are enough basis functions, and the lowest energy -54.073 MeV derived from a single THSR wave function is actually very similar to this result, which also reflects the good approximation of the single THSR wave function.

After the computation above in this section, the required calculation of the THSR and GCM approaches in the real number field for ^{8}Be is complete, and on top of this preparation we can move on to the introduction of the CSM, namely

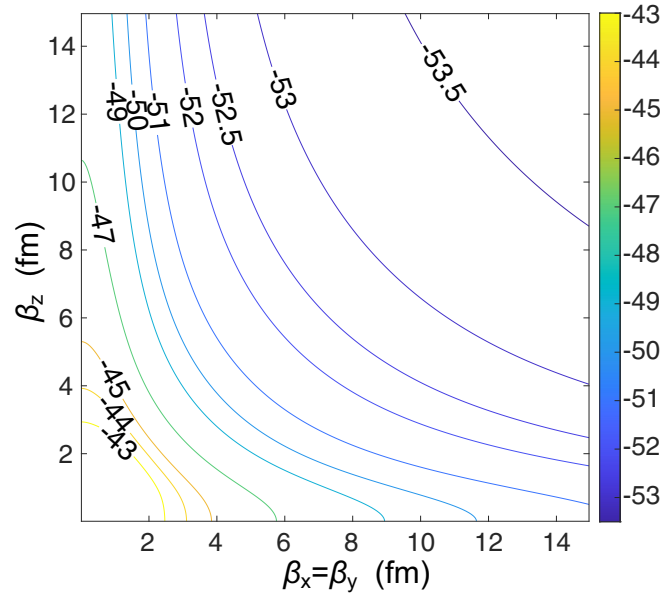

FIG. 4. Contour map of the energy surface of the 4^+ state of ^{8}Be in the two-parameter space, $\beta_x = \beta_y$ and β_z.

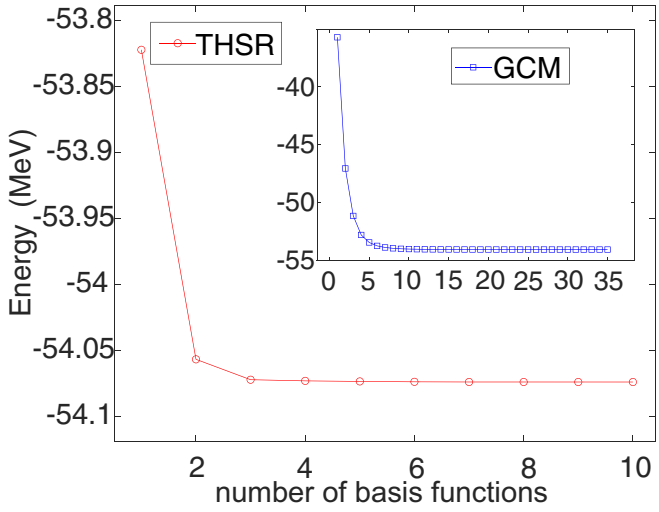

FIG. 5. Energy of the 0^+ state converges to about -54.074 MeV with the increasing basis size of either THSR wave functions or Brink wave functions. The parameters of the ten THSR wave functions are $(\beta_x = \beta_y, \beta_z) = (2,4)$, (2,6), (2,8), (2,10), (2,12), (4,2), (4,6), (4,8), (4,10), (4,12) fm in order, while the parameters of the 35 Brink wave functions are $R = 1, 2, \ldots, 35$ fm in order.

turning to the complex number field. Here we first give the calculation of CSM in the GCM framework and show the calculated resonant state energy. Finally we give the corresponding calculations and results in the THSR framework. For the sake of clarity we will use the 4^+ state as an example below to illustrate the details of the calculation.

The number of the basis functions used in the complex scaled GCM framework is 35, and these generator coordinates R_i $(i = 1, 2, \ldots, 35)$ are spaced evenly in the interval [1, 35] fm. Of course we can choose another distribution of the generator coordinates; however, a test calculation about

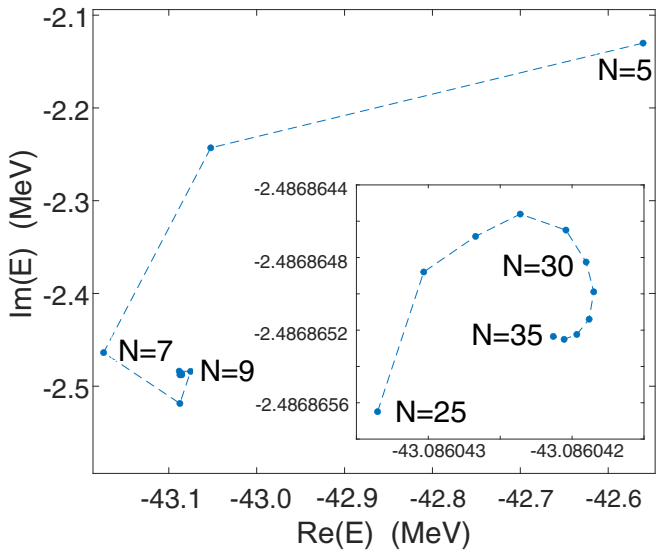

FIG. 6. The N (number of the basis functions) trajectory of the 4^+ resonance energy belonging to the GCM framework with $\theta = 30^\circ$. The generator coordinate R is taken as $1, 2, 3, \ldots, N$ (fm).

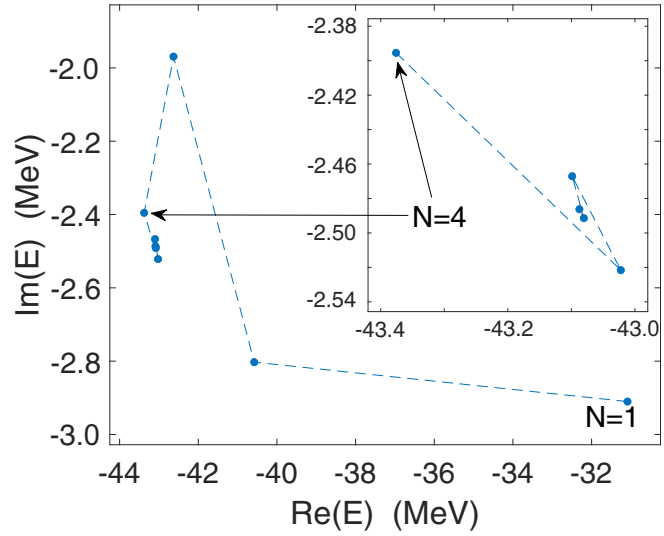

FIG. 7. The N (number of the basis functions) trajectory of the 4^+resonance energy belonging to the THSR framework with $\theta = 30^\circ$. The parameter β_z is fixed to 10^{-6} fm and $\beta_x(=\beta_y)$ is taken as $\frac{\beta_x^2}{b^2} = \frac{1}{10}, 1, 2, 3, \ldots, 7$ in order.

convergence will prove that our choice is appropriate. We fix the value of θ and let the maximum value $R_{\max}$ of the generator coordinate increase from a value less than 35 fm to 35 fm (the generator coordinates are still evenly spaced in the interval $[1, R_{\max}]$ fm) and calculate the resonance energy. As shown in Fig. 6 (for THSR, Fig. 7), the energy will converge with the increase of the number of the basis functions. Using 35 basis functions already meets our needs of accuracy completely,

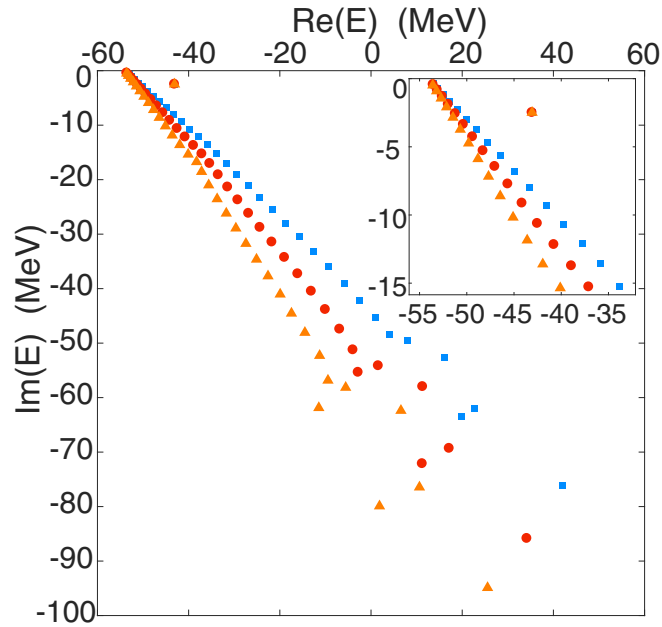

FIG. 8. Complex energy spectrum for the 4^+ state with GCM wave functions. The blue square, red circle, and orange triangle correspond to $\theta = 20^\circ, 23^\circ, 26^\circ$ respectively. It can be seen that the energy values of the resonant state at these three angles basically coincide.

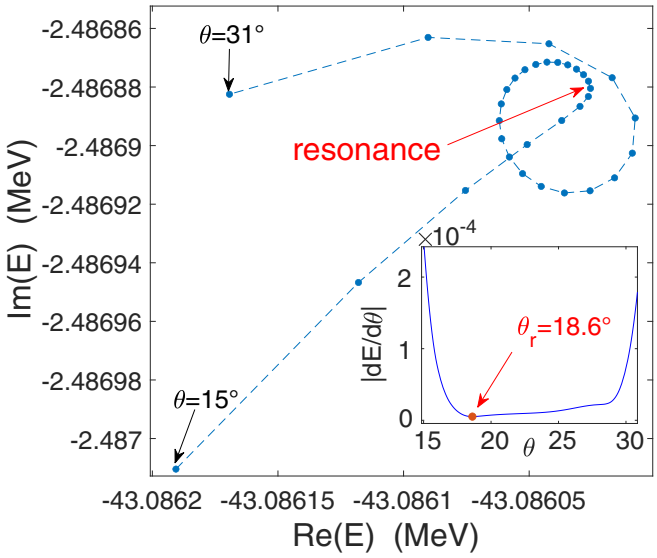

FIG. 9. The θ trajectory with GCM wave functions in the case of the 4^+ state. The generator coordinates are taken as $1, 2, 3, \ldots, 35$ (fm). θ varies from 15° to 31° by steps of 0.5°. The subplot shows the variation of the derivative of the energy with angle. The minimum value is at about $\theta = 18.6^\circ$. The resonance energy at this stabilization point is what we look for.

and we display the complex energy spectrum with different angles in Fig. 8. Now let us determine the precise position and width of the resonance. We fix the number of the basis functions to 35 and draw the trajectory of resonance energy in the complex plane as a function of θ in Fig. 9; it shows that the rate of variation of energy with angle becomes minimum at a certain angle, and the corresponding energy is what we expect. Similarly, for the THSR framework we show the complex energy spectrum with different angles in Fig. 10 and draw the trajectory of resonance energy in the complex plane as a function of θ in Fig. 11.

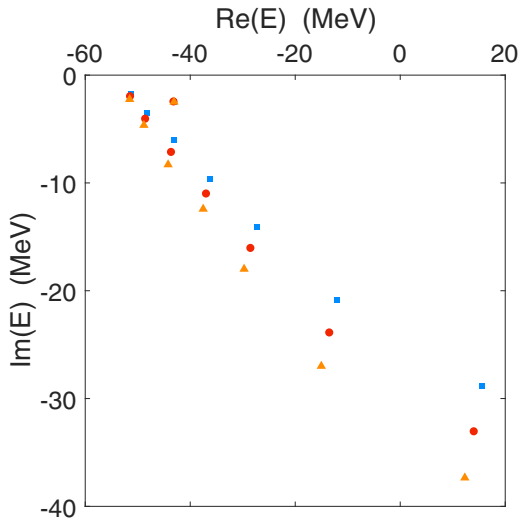

FIG. 10. Complex energy spectrum for the 4^+ state with THSR wave functions. The blue square, red circle, and orange triangle correspond to $\theta = 20^\circ, 23^\circ, 26^\circ$ respectively.

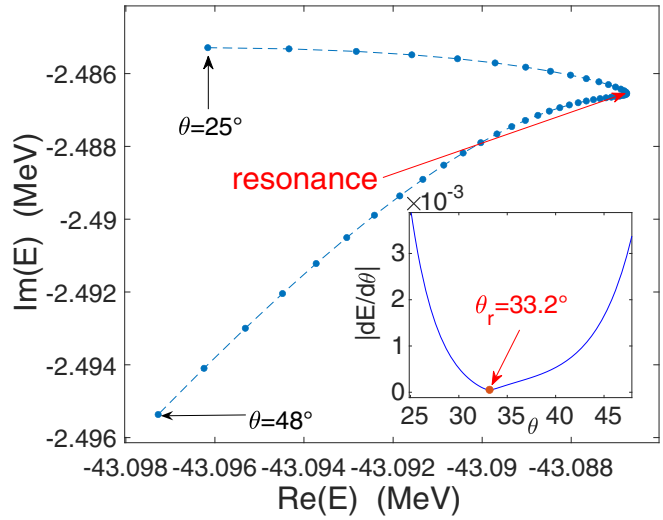

FIG. 11. The θ trajectory with THSR wave functions in the case of the 4^+ state. The parameters are chosen as $\beta_z = 10^{-6}$ fm, $\frac{\beta_x^2}{b^2} = \frac{1}{10}, 1, 2, 3, \ldots, 7$. θ varies from 25° to 48° by steps of 0.5°. The resonance has been marked in the figure.

Using the same procedure, we choose a set of THSR wave functions as basis functions to repeat the calculations above for the 4^+ state.

The advantage of using the THSR wave function is that only fewer basis functions are needed to get almost as good results as the GCM; here we adopt the parameters $\beta_z = 10^{-6}$ fm, $\frac{\beta_x^2}{b^2} = \frac{1}{10}, 1, 2, 3, \ldots, 7$. Fixing β_z and changing only $\beta_x = \beta_y$ is just for illustration and formal clarity, for example we can exchange the two parameters β_z and β_x or take a more complex selection approach instead of fixing a certain parameter, but, no matter how, we can obtain almost the same resonance energy with different selections. Furthermore, the advantage of taking β_z to a value very close to 0 is that it increases the speed of the calculation.

As for the other states the calculation methods are identical and the results are listed in Table I. The result for the 0^+ state is not shown in the table; here we would like to point out that in our approach we cannot get the extremely small resonance width of 0^+ states, whose value measured in the experiment is about 5.57×10^{-6} MeV. But for the broad resonant states we can achieve pretty good accuracy.

IV. CONCLUSIONS

In order to apply the complex scaling method to the microscopic cluster model to solve problems concerning resonant states, we use ^{8}Be as a simple example to illustrate the specific computational details and advantages of this method. This method is a direct approach to solve the position and the width of the resonant state energy simultaneously. We make some changes to the existing code of the cluster model to introduce the complex scale part, which means that for the GCM framework the generation coordinates need to be changed, while for the THSR framework the deformation parameters β need to be changed. Here the complex-scaling rotational operator

TABLE I. The complex energies $E = E_r - i\Gamma/2$ of some resonances of ^{8}Be. The zero of the energy scale is the threshold energy of two-alpha particle, namely −54.17 MeV. The experimental values are taken from NNDC [50].

	Experimental values		GCM		THSR	
L	E_r (MeV)	Γ (MeV)	E_r (MeV)	Γ (MeV)	E_r (MeV)	Γ (MeV)
0	0.0918	5.57×10^{-6}	0.0975		0.0976	
2	3.030	1.513	2.6283	1.2440	2.6237	1.2471
4	11.35	≈3.5	11.0854	4.9738	11.0846	4.9731

acts on the relative coordinate **r** between two α clusters, which means the decay width obtained is the α-cluster decay width rather than the total one. For ^{8}Be this framework is totally available but it may not be suitable for a system without a clear division of cluster components. We would like to point out the this work is our preliminary attempt and we may discuss this problem in more detail in our subsequent work. The computational results show the stability of solutions for broad resonance and the feasibility of extending it to more complex cluster systems.

The wave function used for superposition in this work is either the THSR wave function or the GCM wave function, but we can also choose a hybrid wave function of the THSR and GCM wave functions (hybrid Brink-THSR).

As for the approximation utilized to solve the problem, this work belongs to the stabilization method. It expands the trial wave function in terms of a set of square-integrable basis functions and picks the energy of the resonant state using the stability condition: when the energy of the resonant state varies most slowly with the rotation angle θ, it is the precise determination we expect.

Using the complex scaled THSR wave function, this work could be extended to resonant states of light nuclei that are slightly heavier than ^{8}Be, such as ^{12}C, ^{16}O, and ^{20}Ne, which have more complex cluster structures and energy spectra, but the treatment should remain almost the same as ^{8}Be. For these light nuclei, there have been many advances in recent studies using the THSR wave function; for example, the proposed container model based on the THSR wave function can well explain the rotation band energy spectrum and other information of the light nuclei. Based on these well-established methods and models, it is possible to introduce complex scaling methods for the study of the resonance states with some modifications. A major advantage of this approach is its compatibility with existing cluster model programs, and the original program version can be considered as a special case of the complex scaled one. In addition, it is possible to apply the complex scaling method to heavy and even superheavy nuclei with rich cluster structures, and one possible way may be combining it with the quartet model [51–57] to deal with some alpha cluster problems for heavy and superheavy nuclei.

ACKNOWLEDGMENTS

This work is supported by the National Natural Science Foundation of China (Grants No. 11975167, No. 12035011, No. 11905103, No. 11947211, No. 11761161001, No. 11961141003, and No. 12022517), by the National Key R&D Program of China (Contracts No. 2018YFA0404403 and No. 2016YFE0129300), by the Science and Technology Development Fund of Macau (Grants No. 0048/2020/A1 and No. 008/2017/AFJ), and by the Fundamental Research Funds for the Central Universities (Grant No. 22120210138 and No. 22120200101).

APPENDIX

In the following we give the most general form of the overlap and Hamiltonian kernels, i.e., the deformation parameters $\beta_x(=\beta_y)$ and β_z are not the same in the bra and ket; here we use the $'$ to denote such difference. If the deformation parameters are all the same in the bra and ket then the relevant equations will return to the case of the single THSR wave function. When ζ is 0, we obtain the corresponding kernels of the intrinsic state without the angular momentum projection.

For ^{8}Be the formula of the overlap is

$$\langle \Psi_{2\alpha}(\beta_x = \beta_y, \beta_z)|\hat{R}_y(\zeta)|\Psi_{2\alpha}(\beta'_x = \beta'_y, \beta'_z)\rangle = \int d^3R d^3R' \exp\left[-\left(\sum_{k=x,y,z}\frac{R_k^2}{2\beta_k^2} + \sum_{k=x,y,z}\frac{(R_y(\zeta)\mathbf{R}')_k^2}{2\beta_k'^2}\right)\right] \times \langle \Phi^B(\mathbf{R})|\Phi^B(\mathbf{R}')\rangle$$
$$= (2\pi)^3\beta_x^2\beta_x'^2\beta_z\beta_z'(N_0 + N_1 + N_2), \tag{A1}$$

where

$$N_0 = \frac{2}{\sqrt{\left(\alpha_1^2 + \alpha_1'^2 + 1\right)\left[\left(\alpha_1^2 + \alpha_1'^2 + 1\right)\left(\alpha_2^2 + \alpha_2'^2 + 1\right) + \gamma\right]}},$$

$$N_1 = \frac{-8}{\sqrt{\left(\frac{3}{4}\alpha_1^2\alpha_1'^2 + \alpha_1^2 + \alpha_1'^2 + 1\right)\left[\left(\frac{3}{4}\alpha_1^2\alpha_1'^2 + \alpha_1^2 + \alpha_1'^2 + 1\right)\left(\frac{3}{4}\alpha_2^2\alpha_2'^2 + \alpha_2^2 + \alpha_2'^2 + 1\right) + \frac{\gamma}{4}\right]}},$$

$$N_2 = \frac{6}{\left(\alpha_1^2\alpha_1'^2 + \alpha_1^2 + \alpha_1'^2 + 1\right)\sqrt{\left(\alpha_2^2\alpha_2'^2 + \alpha_2^2 + \alpha_2'^2 + 1\right)}}. \tag{A2}$$

In the above relations, we introduced variables, α_1, α_1', α_2, α_2', and γ, defined as $\alpha_1 = \frac{\beta_x}{b}$, $\alpha_1' = \frac{\beta_x'}{b}$, $\alpha_2 = \frac{\beta_z}{b}$, $\alpha_2' = \frac{\beta_z'}{b}$, $\gamma = (\alpha_1^2 - \alpha_2^2)(\alpha_1'^2 - \alpha_2'^2)\sin^2(\zeta)$. Here we need to note that if $\beta_x(=\beta_y) = \beta_z$ [or $\beta_x'(=\beta_y') = \beta_z'$], then numerically we cannot complete a valid angular momentum projection. However, physically the spin projection state still exists in the equal parameter case, therefore we can make the limiting procedure of $\beta_x(=\beta_y) \to \beta_z$ to numerically calculate.

The formula of the kinetic energy is obtained by using the relation

$$\left\langle \Phi^B(\mathbf{R})|T - T_G|\Phi^B(\mathbf{R}')\right\rangle = \frac{\hbar}{mb^2}\left(\frac{3}{4}(A-1) + \frac{\nu}{2}\frac{d}{d\nu}\right)\langle\Phi^B(\mathbf{R})|\Phi^B(\mathbf{R}')\rangle, \tag{A3}$$

where $\nu = \frac{1}{2b^2}$ and A is the nucleon number of ^{8}Be. Thus the formula of the kinetic energy is

$$\begin{aligned}
&\langle\Psi_{2\alpha}(\beta_x = \beta_y, \beta_z)|(T - T_G)\hat{R}_y(\zeta)|\Psi_{2\alpha}(\beta_x' = \beta_y', \beta_z')\rangle \\
&= \int d^3R d^3R' \exp\left[-\left(\sum_{k=x,y,z}\frac{R_k^2}{2\beta_k^2} + \sum_{k=x,y,z}\frac{(R_y(\zeta)\mathbf{R}')_k^2}{2\beta_k'^2}\right)\right] \times \langle\Phi^B(\mathbf{R})|T - T_G|\Phi^B(\mathbf{R}')\rangle \\
&= (2\pi)^3\beta_x^2\beta_x'^2\beta_z\beta_z'\frac{\hbar}{mb^2}\left\{\frac{21}{4}(N_0 + N_1 + N_2) - \frac{N_0}{4}\left[\frac{3\left(\alpha_1^2 + \alpha_1'^2\right) + 2}{\alpha_1^2 + \alpha_1'^2 + 1} - \frac{\alpha_1^2 + \alpha_1'^2 + 1 + \alpha_2^2 + \alpha_2'^2 + 1}{\left(\alpha_1^2 + \alpha_1'^2 + 1\right)\left(\alpha_2^2 + \alpha_2'^2 + 1\right) + \gamma}\right]\right. \\
&\quad - \frac{N_1}{4}\left[\frac{3\alpha_1^2\alpha_1'^2 + 3\left(\alpha_1^2 + \alpha_1'^2\right) + 2}{\frac{3}{4}\alpha_1^2\alpha_1'^2 + \alpha_1^2 + \alpha_1'^2 + 1} + \frac{\left(\frac{3}{4}\alpha_2^2\alpha_2'^2 - 1\right)\left(\frac{3}{4}\alpha_1^2\alpha_1'^2 + \alpha_1^2 + \alpha_1'^2 + 1\right)}{\left(\frac{3}{4}\alpha_1^2\alpha_1'^2 + \alpha_1^2 + \alpha_1'^2 + 1\right)\left(\frac{3}{4}\alpha_2^2\alpha_2'^2 + \alpha_2^2 + \alpha_2'^2 + 1\right) + \frac{\gamma}{4}}\right. \\
&\quad \left.\left. + \frac{\left(\frac{3}{4}\alpha_1^2\alpha_1'^2 - 1\right)\left(\frac{3}{4}\alpha_2^2\alpha_2'^2 + \alpha_2^2 + \alpha_2'^2 + 1\right)}{\left(\frac{3}{4}\alpha_1^2\alpha_1'^2 + \alpha_1^2 + \alpha_1'^2 + 1\right)\left(\frac{3}{4}\alpha_2^2\alpha_2'^2 + \alpha_2^2 + \alpha_2'^2 + 1\right) + \frac{\gamma}{4}}\right] - \frac{N_2}{4}\left(2\frac{2\alpha_1^2\alpha_1'^2 + \alpha_1^2 + \alpha_1'^2}{\alpha_1^2\alpha_1'^2 + \alpha_1^2 + \alpha_1'^2 + 1} + \frac{2\alpha_2^2\alpha_2'^2 + \alpha_2^2 + \alpha_2'^2}{\alpha_2^2\alpha_2'^2 + \alpha_2^2 + \alpha_2'^2 + 1}\right)\right\}.
\end{aligned} \tag{A4}$$

In this work we make use of the Volkov interactions as the two-body force, so V_N reads as follows:

$$V_N = \frac{1}{2}\sum_{i\neq j}^{8}\{(1-M) - MP_\sigma P_\tau\}_{ij}\sum_{n=1}^{2}V_n\exp\left(-\frac{r_{ij}^2}{a_n^2}\right). \tag{A5}$$

Here we adopt Volkov No. 1 interaction, and the parameters V_n and a_n are $a_1 = 1.60$ fm, $a_2 = 0.82$ fm, $V_1 = -83.34$ MeV, $V_2 = 144.86$ MeV. In the following formula we used the variables defined as $X_d = 8 - 10M$, $X_e = 10M - 2$, $U_n = \frac{b^2}{a_n^2 + 2b^2}$. The formula of the two-body nuclear interaction energy is as follows:

$$\begin{aligned}
&\langle\Psi_{2\alpha}(\beta_x = \beta_y, \beta_z)|V_N\hat{R}_y(\zeta)|\Psi_{2\alpha}(\beta_x' = \beta_y', \beta_z')\rangle \\
&= \int d^3R d^3R' \exp\left[-\left(\sum_{k=x,y,z}\frac{R_k^2}{2\beta_k^2} + \sum_{k=x,y,z}\frac{(R_y(\zeta)\mathbf{R}')_k^2}{2\beta_k'^2}\right)\right] \times \langle\Phi^B(\mathbf{R})|V_N|\Phi^B(\mathbf{R}')\rangle \\
&= (2\pi)^3\beta_x^2\beta_x'^2\beta_z\beta_z'\sum_{n=1}^{2}V_n\left(\frac{a_n^2}{a_n^2 + 2b^2}\right)^{3/2}\left[4(X_d + X_e)\left(\frac{N_0}{2} + \frac{N_1}{4} + \frac{N_2}{6}\right) + \frac{4X_d}{\sqrt{2U_n\alpha_1^2\alpha_1'^2 + \left(1 + \frac{U_n}{2}\right)\left(\alpha_1^2 + \alpha_1'^2\right) + 1}}\right. \\
&\quad \times \frac{1}{\sqrt{\left[2U_n\alpha_1^2\alpha_1'^2 + \left(1 + \frac{U_n}{2}\right)\left(\alpha_1^2 + \alpha_1'^2\right) + 1\right]\left[2U_n\alpha_2^2\alpha_2'^2 + \left(1 + \frac{U_n}{2}\right)\left(\alpha_2^2 + \alpha_2'^2\right) + 1\right] + \left(U_n - 2\right)^2\frac{\gamma}{4}}} \\
&\quad + \frac{4X_e}{\sqrt{\left(\frac{U_n}{2} + \frac{3}{4}\right)\alpha_1^2\alpha_1'^2 + \left(1 + \frac{U_n}{2}\right)\left(\alpha_1^2 + \alpha_1'^2\right) + 1}} \\
&\quad \times \frac{1}{\sqrt{\left[\left(\frac{U_n}{2} + \frac{3}{4}\right)\alpha_1^2\alpha_1'^2 + \left(1 + \frac{U_n}{2}\right)\left(\alpha_1^2 + \alpha_1'^2\right) + 1\right]\left[\left(\frac{U_n}{2} + \frac{3}{4}\right)\alpha_2^2\alpha_2'^2 + \left(1 + \frac{U_n}{2}\right)\left(\alpha_2^2 + \alpha_2'^2\right) + 1\right] + \left(U_n + 1\right)^2\frac{\gamma}{4}}} \\
&\quad \left. + \frac{4(X_e - 2X_d)}{\sqrt{\left(\frac{3U_n}{2} + \frac{3}{4}\right)\alpha_1^2\alpha_1'^2 + \left(1 + \frac{U_n}{2}\right)\left(\alpha_1^2 + \alpha_1'^2\right) + 1}}\right]
\end{aligned}$$

$$
\begin{aligned}
&\times \frac{1}{\sqrt{\left[\left(\frac{3U_n}{2}+\frac{3}{4}\right)\alpha_1^2\alpha_1'^2+\left(1+\frac{U_n}{2}\right)\left(\alpha_1^2+\alpha_1'^2\right)+1\right]\left[\left(\frac{3U_n}{2}+\frac{3}{4}\right)\alpha_2^2\alpha_2'^2+\left(1+\frac{U_n}{2}\right)\left(\alpha_2^2+\alpha_2'^2\right)+1\right]+\left(U_n-1\right)^2\frac{\gamma}{4}}}\\
&+\frac{4(X_d-2X_e)}{\sqrt{\left(U_n+1\right)\alpha_1^2\alpha_1'^2+\left(1+\frac{U_n}{2}\right)\left(\alpha_1^2+\alpha_1'^2\right)+1}}\\
&\times \frac{1}{\sqrt{\left[\left(U_n+1\right)\alpha_1^2\alpha_1'^2+\left(1+\frac{U_n}{2}\right)\left(\alpha_1^2+\alpha_1'^2\right)+1\right]\left[\left(U_n+1\right)\alpha_2^2\alpha_2'^2+\left(1+\frac{U_n}{2}\right)\left(\alpha_2^2+\alpha_2'^2\right)+\right]+U_n^2\frac{\gamma}{4}}}\\
&-\frac{8(X_d+X_e)}{\sqrt{\left(\frac{U_n}{2}+\frac{3}{4}\right)\alpha_1^2\alpha_1'^2+\left(1+\frac{U_n}{2}\right)\alpha_1^2+\alpha_1'^2+1}}\\
&\times \frac{1}{\sqrt{\left[\left(\frac{U_n}{2}+\frac{3}{4}\right)\alpha_1^2\alpha_1'^2+\left(1+\frac{U_n}{2}\right)\alpha_1^2+\alpha_1'^2+1\right]\left[\left(\frac{U_n}{2}+\frac{3}{4}\right)\alpha_2^2\alpha_2'^2+\left(1+\frac{U_n}{2}\right)\alpha_2^2+\alpha_2'^2+1\right]+\frac{\gamma}{4}}}\\
&-\frac{8(X_d+X_e)}{\sqrt{\left(\frac{U_n}{2}+\frac{3}{4}\right)\alpha_1^2\alpha_1'^2+\left(1+\frac{U_n}{2}\right)\alpha_1'^2+\alpha_1^2+1}}\\
&\times \frac{1}{\sqrt{\left[\left(\frac{U_n}{2}+\frac{3}{4}\right)\alpha_1^2\alpha_1'^2+\left(1+\frac{U_n}{2}\right)\alpha_1'^2+\alpha_1^2+1\right]\left[\left(\frac{U_n}{2}+\frac{3}{4}\right)\alpha_2^2\alpha_2'^2+\left(1+\frac{U_n}{2}\right)\alpha_2'^2+\alpha_2^2+1\right]+\frac{\gamma}{4}}}\\
&+\frac{8(X_d+X_e)}{\sqrt{\left(\frac{U_n}{2}+1\right)\alpha_1^2\alpha_1'^2+\left(1+\frac{U_n}{2}\right)\alpha_1^2+\alpha_1'^2+1}}\\
&\times \frac{1}{\sqrt{\left[\left(\frac{U_n}{2}+1\right)\alpha_1^2\alpha_1'^2+\left(1+\frac{U_n}{2}\right)\alpha_1^2+\alpha_1'^2+1\right]\left[\left(\frac{U_n}{2}+1\right)\alpha_2^2\alpha_2'^2+\left(1+\frac{U_n}{2}\right)\alpha_2^2+\alpha_2'^2+1\right]}}\\
&+\frac{8(X_d+X_e)}{\sqrt{\left(\frac{U_n}{2}+1\right)\alpha_1^2\alpha_1'^2+\left(1+\frac{U_n}{2}\right)\alpha_1'^2+\alpha_1^2+1}}\\
&\times \frac{1}{\sqrt{\left[\left(\frac{U_n}{2}+1\right)\alpha_1^2\alpha_1'^2+\left(1+\frac{U_n}{2}\right)\alpha_1'^2+\alpha_1^2+1\right]\left[\left(\frac{U_n}{2}+1\right)\alpha_2^2\alpha_2'^2+\left(1+\frac{U_n}{2}\right)\alpha_2'^2+\alpha_2^2+1\right]}}\Bigg].
\end{aligned}
\tag{A6}
$$

As for the Coulomb interaction energy, we represent it as a superposition of Gaussian functions:

$$
V_C=\frac{1}{2}\sum_{i\neq j}^{8}\left(\frac{1}{2}+t_{zi}\right)\left(\frac{1}{2}+t_{zj}\right)\frac{e^2}{r_{ij}}=\frac{1}{2}\sum_{i\neq j}^{8}\left(\frac{1}{2}+t_{zi}\right)\left(\frac{1}{2}+t_{zj}\right)\frac{2e^2}{\sqrt{\pi}}\int_0^\infty d\eta\exp\left(-r_{ij}^2\eta^2\right). \tag{A7}
$$

Using this equation we can obtain the matrix elements of Coulomb interaction by changing the variables used in V_N in the following way:

$$
\begin{aligned}
a_n^2 &\longrightarrow \frac{1}{\eta^2},\\
\sum_{n=1}^{2}V_n\left(\frac{a_n^2}{a_n^2+2b^2}\right)^{3/2} &\longrightarrow \frac{2e^2}{\sqrt{\pi}}\int_0^\infty\left(\frac{1}{1+2b^2\eta^2}\right)^{3/2}d\eta,\\
X_d &\longrightarrow 2,\\
X_e &\longrightarrow -1.
\end{aligned}
\tag{A8}
$$

It is convenient to use a new variable ξ (the range of integration over ξ is from 0 to 1) in the integration:

$$
\begin{aligned}
\xi^2&=\frac{2b^2\eta^2}{1+2b^2\eta^2},\\
\sqrt{\frac{1}{2b^2}}d\xi&=\left(\frac{1}{1+2b^2\eta^2}\right)^{3/2}d\eta.
\end{aligned}
\tag{A9}
$$

The kernels obtained above can be integrated with the weight of $P_J(\cos(\zeta))$ to obtain the corresponding kernels after the angular momentum projection. The integration in this step can be calculated directly by the analytical method or solved numerically.

[1] A. Tohsaki, H. Horiuchi, P. Schuck, and G. Röpke, Alpha Cluster Condensation in ^{12}C and ^{16}O, Phys. Rev. Lett. **87**, 192501 (2001).

[2] Y. Funaki, H. Horiuchi, and A. Tohsaki, Cluster models from RGM to alpha condensation and beyond, Prog. Part. Nucl. Phys. **82**, 78 (2015).

[3] P. Schuck, Y. Funaki, H. Horiuchi, G. Röpke, A. Tohsaki, and T. Yamada, Alpha particle clusters and their condensation in nuclear systems, Phys. Scr. **91**, 123001 (2016).

[4] A. Tohsaki, H. Horiuchi, P. Schuck, and G. Röpke, Status of α-particle condensate structure of the Hoyle state, Rev. Mod. Phys. **89**, 011002 (2017).

[5] M. Freer, H. Horiuchi, Y. Kanada-En'yo, D. Lee, and U. G. Meißner, Microscopic clustering in light nuclei, Rev. Mod. Phys. **90**, 035004 (2018).

[6] B. Zhou, Y. Funaki, H. Horiuchi, and A. Tohsaki, Nonlocalized clustering and evolution of cluster structure in nuclei, Front. Phys. (Beijing) **15**, 14401 (2020).

[7] M. Lyu, K. Yoshida, Y. Kanada-En'yo, and K. Ogata, Manifestation of α clustering in ^{10}Be via α-knockout reaction, Phys. Rev. C **97**, 044612 (2018).

[8] Y. Funaki, H. Horiuchi, A. Tohsaki, P. Schuck, and G. Röpke, Description of ^{8}Be as deformed gas-like two-alpha-particle states, Prog. Theor. Phys. **108**, 297 (2002).

[9] Y. Funaki, H. Horiuchi, W. von Oertzen, G. Röpke, P. Schuck, A. Tohsaki, and T. Yamada, Concepts of nuclear alpha-particle condensation, Phys. Rev. C **80**, 064326 (2009).

[10] M. Lyu, Z. Ren, B. Zhou, Y. Funaki, H. Horiuchi, G. Röpke, P. Schuck, A. Tohsaki, C. Xu, and T. Yamada, Investigation of ^{9}Be from nonlocalized clustering concept, Phys. Rev. C **91**, 014313 (2015).

[11] M. Lyu, Z. Ren, B. Zhou, Y. Funaki, H. Horiuchi, G. Röpke, P. Schuck, A. Tohsaki, C. Xu, and T. Yamada, Investigation of ^{10}Be and its cluster dynamics with the nonlocalized clustering approach, Phys. Rev. C **93**, 054308 (2016).

[12] M. Lyu, Z. Ren, H. Horiuchi, B. Zhou, Y. Funaki, G. Röpke, P. Schuck, A. Tohsaki, C. Xu, and T. Yamada, Properties of $^{8-11}$Be isotopes with isospin-dependent spin–orbit potential in a cluster approach, Eur. Phys. J. A **57**, 51 (2021).

[13] Q. Zhao, Z. Ren, M. Lyu, H. Horiuchi, Y. Funaki, G. Röpke, P. Schuck, A. Tohsaki, C. Xu, T. Yamada *et al.*, Investigation of the ^{9}B nucleus and its cluster-nucleon correlations, Phys. Rev. C **97**, 054323 (2018).

[14] Q. Zhao, Z. Ren, M. Lyu, H. Horiuchi, Y. Kanada-En'yo, Y. Funaki, G. Röpke, P. Schuck, A. Tohsaki, C. Xu *et al.*, Investigation of isospin-triplet and isospin-singlet pairing in the $A = 10$ nuclei ^{10}B, ^{10}Be, and ^{10}C with an extension of the Tohsaki-Horiuchi-Schuck-Röpke wave function, Phys. Rev. C **100**, 014306 (2019).

[15] T. Suhara, Y. Funaki, B. Zhou, H. Horiuchi, and A. Tohsaki, One-Dimensional α Condensation of α-Linear-Chain States in ^{12}C and ^{16}O, Phys. Rev. Lett. **112**, 062501 (2014).

[16] B. Zhou, Y. Funaki, A. Tohsaki, H. Horiuchi, and Z. Ren, The container picture with two-alpha correlation for the ground state of ^{12}C, Prog. Theor. Exp. Phys. **2014**, 101D01 (2014).

[17] B. Zhou, A. Tohsaki, H. Horiuchi, and Z. Ren, Breathing-like excited state of the Hoyle state in ^{12}C, Phys. Rev. C **94**, 044319 (2016).

[18] N. Itagaki, H. Matsuno, and A. Tohsaki, Explicit inclusion of the spin-orbit contribution in the Tohsaki-Horiuchi-Schuck-Röpke wave function, Phys. Rev. C **98**, 044306 (2018).

[19] B. Zhou, Y. Funaki, H. Horiuchi, M. Kimura, Z. Ren, G. Röpke, P. Schuck, A. Tohsaki, C. Xu, and T. Yamada, Nonlocalized motion in a two-dimensional container of α particles in 3^- and 4^- states of ^{12}C, Phys. Rev. C **99**, 051303(R) (2019).

[20] Y. Funaki, "Container" evolution for cluster structures in ^{16}O, Phys. Rev. C **97**, 021304(R) (2018).

[21] B. Zhou, Z. Ren, C. Xu, Y. Funaki, T. Yamada, A. Tohsaki, H. Horiuchi, P. Schuck, and G. Röpke, New concept for the ground-state band in ^{20}Ne within a microscopic cluster model, Phys. Rev. C **86**, 014301 (2012).

[22] B. Zhou, Y. Funaki, H. Horiuchi, Z. Ren, G. Röpke, P. Schuck, A. Tohsaki, C. Xu, and T. Yamada, Nonlocalized Clustering: A New Concept in Nuclear Cluster Structure Physics, Phys. Rev. Lett. **110**, 262501 (2013).

[23] B. Zhou, Y. Funaki, H. Horiuchi, Z. Ren, G. Röpke, P. Schuck, A. Tohsaki, C. Xu, and T. Yamada, Nonlocalized cluster dynamics and nuclear molecular structure, Phys. Rev. C **89**, 034319 (2014).

[24] B. Zhou, New trial wave function for the nuclear cluster structure of nuclei, Prog. Theor. Exp. Phys. **2018**, 041D01 (2018).

[25] T. Myo, Y. Kikuchi, H. Masui, and K. Katō, Recent development of complex scaling method for many-body resonances and continua in light nuclei, Prog. Part. Nucl. Phys. **79**, 1 (2014).

[26] D. Baye and P. H. Heenen, Microscopic R-Matrix theory in a generator coordinate basis: (I). Theory and application to dineutron-dineutron and $\alpha\alpha$ scattering, Nucl. Phys. A **233**, 304 (1974).

[27] P. H. Heenen, Microscopic R-matrix theory in a generator coordinate basis, Nucl. Phys. A **272**, 399 (1976).

[28] D. Baye, P. H. Heenen, and M. Libert-Heinemann, Microscopic R-matrix theory in a generator coordinate basis, Nucl. Phys. A **291**, 230 (1977).

[29] P. Descouvemont and D. Baye, The R-matrix theory, Rep. Prog. Phys. **73**, 036301 (2010).

[30] D. Bai and Z. Ren, Resonant and scattering states in the $\alpha + \alpha$ system from the nonlocalized cluster model, Phys. Rev. C **101**, 034311 (2020).

[31] Y. Funaki, A. Tohsaki, H. Horiuchi, P. Schuck, and G. Röpke, Resonance states in ^{12}C and alpha-particle condensation, Eur. Phys. J. A **24**, 321 (2005)

[32] Y. Funaki, H. Horiuchi, and A. Tohsaki, New treatment of resonances with bound state approximation by using pseudo potential, Prog. Theor. Phys. **115**, 115 (2006).

[33] S. Okai and S. C. Park, Cluster-model calculation for phase shifts of alpha-alpha scattering, Phys. Rev. **145**, 787 (1966).

[34] D. R. Thompson, M. Lemere, and Y. C. Tang, Systematic investigation of scattering problems with the resonating-group method, Nucl. Phys. A **286**, 53 (1977).

[35] H. Horiuchi, Generator coordinate treatment of composite particle reaction and molecule-like structures, Prog. Theor. Phys. **43**, 375 (1970).

[36] D. Baye and M. Kruglanski, $\alpha + \alpha$ scattering in a microscopic model with monopolar distortion, Phys. Rev. C **45**, 1321 (1992).

[37] R. Higa, H. W. Hammer, and U. van Kolck, $\alpha\alpha$ scattering in halo effective field theory, Nucl. Phys. A **809**, 171 (2008).

[38] P. Andreatta, C. A. Manzata, C. Ji, W. Leidemann, and G. Orlandini, Beryllium-9 in cluster effective field theory, in recent progress in few-body physics, in *Proceedings of the 22nd International Conference on Few-Body Problems in Physics*, edited by N. A. Orr, M. Ploszajczak, F. M. Marqués, and J. Carbonell, Springer Proceedings in Physics Vol. 238 (Springer, Cham, 2020), p. 191.

[39] A. T. Kruppa, R. G. Lovas, and B. Gyarmati, Complex scaling in the cluster model: Resonances in ^{8}Be, Phys. Rev. C **37**, 383 (1988).

[40] E. Garrido, A. S. Jensen, and D. V. Fedorov, Inelastic cross sections and continuum transitions illustrated by ^{8}Be results, Phys. Rev. C **86**, 064608 (2012).

[41] E. Garrido, A. S. Jensen, and D. V. Fedorov, Rotational bands in the continuum illustrated by ^{8}Be results, Phys. Rev. C **88**, 024001 (2013).

[42] E. Garrido, A. S. Jensen, and D. V. Fedorov, Techniques to treat the continuum applied to electromagnetic transitions in ^{8}Be, Few Body Syst. **55**, 101 (2014).

[43] A. B. Volkov, Equilibrium deformation calculations of the ground state energies of 1p shell nuclei, Nucl. Phys. **74**, 33 (1965)

[44] J. Aguilar and J. M. Combes, A class of analytic perturbations for one-body Schrödinger Hamiltonians, Commun. Math. Phys. **22**, 269 (1971).

[45] E. Balslev and J. M. Combes, Spectral properties of many-body Schrödinger operators with dilatation-analytic interactions, Commun. Math. Phys. **22**, 280 (1971).

[46] T. Berggren, On the use of resonant states in eigenfunction expansions of scattering and reaction amplitudes, Nucl. Phys. A **109**, 265 (1968).

[47] N. Michel, W. Nazarewicz, M. Ploszajczak, and T. Vertse, Shell model in the complex energy plane, J. Phys. G: Nucl. Part. Phys. **36**, 013101 (2009).

[48] E. Brändas and P. Froelich, Continuum orbitals, complex scaling problem, and the extended virial theorem, Phys. Rev. A **16**, 2207 (1977).

[49] N. Moiseyev, *Non-Hermitian Quantum Mechanics* (Cambridge University Press, Cambridge, 2011).

[50] https://www.nndc.bnl.gov/nudat3/.

[51] D. Bai and Z. Ren, Woods-Saxon-Gaussian potential and alpha-cluster structures of alpha + closed shell nuclei, Chin. Phys. C **42**, 124102 (2018).

[52] D. Bai and Z. Ren, Cluster-daughter overlap as a new probe of alpha-cluster formation in medium-mass and heavy even–even nuclei, Phys. Lett. B **786**, 5 (2018).

[53] D. Bai, Z. Ren, and G. Röpke, α clustering from the quartet model, Phys. Rev. C **99**, 034305 (2019).

[54] G. Röpke, P. Schuck, B. Zhou, Y. Funaki, H. Horiuchi, Z. Ren, A. Tohsaki, C. Xu, and T. Yamada, Nuclear clusters bound to doubly magic nuclei: The case of ^{212}Po, Phys. Rev. C **90**, 034304 (2014).

[55] C. Xu, Z. Ren, G. Röpke, P. Schuck, Y. Funaki, H. Horiuchi, A. Tohsaki, T. Yamada, and B. Zhou, α-decay width of ^{212}Po from a quartetting wave function approach, Phys. Rev. C **93**, 011306(R) (2016).

[56] C. Xu, G. Röpke, P. Schuck, Z. Ren, Y. Funaki, H. Horiuchi, A. Tohsaki, T. Yamada, and B. Zhou, α-cluster formation and decay in the quartetting wave function approach, Phys. Rev. C **95**, 061306(R) (2017).

[57] G. Röpke, P. Schuck, Y. Funaki, H. Horiuchi, Z. Ren, A. Tohsaki, C. Xu, T. Yamada, and B. Zhou, Alpha decay width of ^{212}Po from a quartetting wave function approach, J. Phys.: Conf. Ser. **863**, 012006 (2017).